

RapidVol: Rapid Reconstruction of 3D Ultrasound Volumes from Sensorless 2D Scans

Mark C. Eid^{1,2,*} Pak-Hei Yeung² Madeleine K. Wyburd²
João F. Henriques¹ Ana I.L. Namburete²

¹Visual Geometry Group, University of Oxford

²Oxford Machine Learning in NeuroImaging Lab, University of Oxford

*markeid@robots.ox.ac.uk

Abstract

Two-dimensional (2D) freehand ultrasonography is one of the most commonly used medical imaging modalities, particularly in obstetrics and gynaecology. However, it only captures 2D cross-sectional views of inherently 3D anatomies, losing valuable contextual information. As an alternative to requiring costly and complex 3D ultrasound scanners, 3D volumes can be constructed from 2D scans using machine learning. However this usually requires long computational time. Here, we propose RapidVol: a neural representation framework to speed up slice-to-volume ultrasound reconstruction. We use *tensor-rank decomposition*, to decompose the typical 3D volume into sets of tri-planes, and store those instead, as well as a small neural network. A set of 2D ultrasound scans, with their ground truth (or estimated) 3D position and orientation (pose) is all that is required to form a complete 3D reconstruction. Reconstructions are formed from real fetal brain scans, and then evaluated by requesting novel cross-sectional views. When compared to prior approaches based on fully implicit representation (e.g. neural radiance fields), our method is over 3x quicker, 46% more accurate, and if given inaccurate poses is more robust. Further speed-up is also possible by reconstructing from a structural prior rather than from scratch.

Keywords: 3D Reconstruction • Ultrasound • Tensor Decomposition • NeRF

1 Introduction

Two-dimensional (2D) freehand ultrasonography is routinely used in prenatal checkups, as well as to image other organs. It is affordable, provides instant visualisation, can be repeated numerously due to lack of ionising radiation, and can even be carried out from a smartphone. However, whilst magnetic resonance imaging (MRI) and computerised tomography (CT) scans capture and store inherently 3D structures within the body as 3D volumes, the same is not true for freehand ultrasound (US). Three-dimensional (3D) US scans do exist, and have several clinical benefits over 2D methods, such as improved detection of cleft lip [1,6,8], and providing greater diagnostic accuracy irrespective of sonographer experience [10,17]. One study quantified this as a 60.8% improvement [11]. To acquire these 3D US scans, native 3D scanners can be used, however they are still not routinely used as they are ~ 10 times more expensive than standard US probes and are bulkier [24]. Operators also require additional training.

An alternative to moving to 3D scanners, is to reconstruct 3D volumes from 2D freehand US scans, acquired from standard sensorless probes. Yeung. et al. [24] proposed a framework, ImplicityVol, to implicitly construct a 3D volume of a fetal brain using a series of freehand 2D US scans, which can also be applied to scans of other fetal or adult organs. Currently, ImplicityVol [24] takes $O(\text{hours})$ to reconstruct a 3D brain, however ideally this would be of $O(\text{minutes})$ so that acquisition *and* reconstruction (as well as analysis of it by a clinician) can take place together within the same appointment. **This paper therefore presents a new representation method, termed RapidVol, which is significantly more accurate (up to 46%), and forms the reconstructed 3D brain from inputted 2D freehand ultrasound scans 3 times quicker.**

2 Preliminary

Traditionally, 3D scenes are represented purely *explicitly*, where the entire 3D volume/scene is stored as a grid of voxels [18,20]. More lightweight versions can use sparse or octree voxel grids, or meshes [19]. A modern technique is to instead store the scene *implicitly*, by saving a fully trained neural network [7,9,12,26]. More recently, hybrid methods have been proposed, combining and drawing upon the benefits of both pure explicit and implicit representation [3,4,21,25].

Explicit Representation: The 3D brain can be represented discretely as a cost volume $\mathbf{V} \in R^{H \times W \times D \times C}$, a tensor of height H , width W , depth D and channels C . A 3D US volume will have $C = 1$ as US is a grayscale modality, colour objects will have $C = 3$. If there are any voxels which were not seen in any of the 2D images used for reconstruction, tri-linear interpolation, nearest neighbour, or spline fitting can be used to predict these missing voxel values [5,13].

Implicit Representation: Based on NeRF [12], ImplicitVol [24] instead represents the 3D brain volume $\mathbf{V} \in \mathbb{R}^{H \times W \times D \times 1}$ as a trainable deep neural network, $F_{\Theta} : \mathbf{x} \rightarrow c$, where Θ denotes the learnable parameters, \mathbf{x} the (x, y, z) co-ordinates of any point within the 3D brain, and c the intensity value. By predicting intensity c at a given input voxel location \mathbf{x} , the discrepancy between c and the actual intensity at \mathbf{x} can be computed as the loss to then update Θ through back-propagation.

Hybrid Implicit-Explicit Representation: Implicit and explicit representation models have contrasting benefits and limitations. For example, explicit models scale *cubically* with resolution, but are quicker to train. Recent works such as TensorRF [4] and EG3D [3] attempt to bridge these two approaches and harness the benefits of both. As shown in Fig. 1, they use tensor rank decomposition to instead store the $H \times W \times D \times C$ cost volume much more compactly as C sets of three 1D Vectors (CP Decomposition [2]), or C sets of three 2D planes (“Tri-Planar Decomposition”) as in EG3D. Only a very small MLP is then needed to decode from C channels to 1/3 colour channel(s). By using a mix of explicit and implicit representation techniques, storage reduces from $O(n^3)$ to $O(n^2)$ and $O(n)$ for Tri-Planar and CP Decomposition respectively. More importantly, the speed benefits associated with explicit representation are still maintained, and in CP Decomposition it is improved (as for each training image, $(H + W)$ rather than $(H \times W)$ parameters have to now be updated). Linear and bilinear interpolation can also be quickly applied within each individual 1D vector (CP Decomposition) or 2D plane (Tri-Planar Decomposition). This compensates for the lack of continuity when using pure explicit representation.

We thus adapt TensorRF [4] and EG3D [3] from the original natural scene setting to the medical imaging setting, specifically on fetal brains. Challenges that must be addressed include the relative lack of training data, the much higher intricacies present in the brain as opposed to the Synthetic-NeRF dataset [12], and the need for high accuracy and interpretability for clinical deployment.

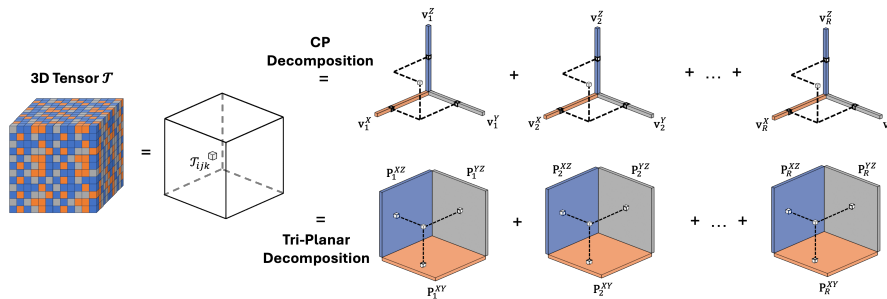


Figure 1: Diagram showing the two different types of tensor decomposition employed, and how the value of a voxel in \mathcal{T} can be retrieved.

3 Methodology

3.1 Problem Setup

In a medical setting, we have a stack Π of N 2D ultrasound images ($\Pi = \{\mathbf{I}_i\}_{i=1}^N$), all of which are different cross-sections but of the same inherently 3D fetal brain (see Fig. 2). Each cross-sectional image has a known pose Λ_i relative to the centre of the 3D brain, which can be parameterised by 3 Euler angles (\mathbf{E}) and 3 Translations (\mathbf{T}). Our goal is to reconstruct the 3D brain such that a 2D cross-section can be viewed at any specified pose Λ , and at any resolution. The final output of RapidVol *appears* to be a high-resolution cost volume \mathbf{V} , however it is actually a set of tri-planes or tri-vectors, and a small MLP.

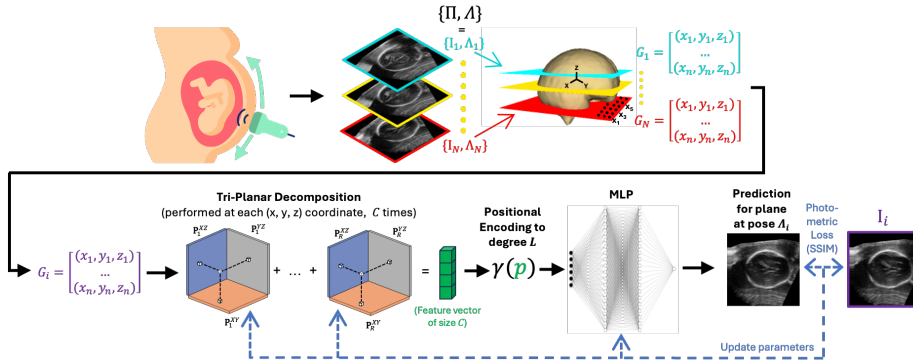


Figure 2: Pipeline of our proposed method RapidVol. During the reconstruction process, a set of Π images and their corresponding poses Λ are required as input. Once the brain is reconstructed, only the pose Λ at which one wishes to see is required as input, and parameters are not updated.

Nb. Ultrasound probe image adapted from Flaticon.com.

3.2 Tensor Decompositions

Tri-Planar Decomposition: Given a 3D Tensor $\mathcal{T} \in \mathbb{R}^{I \times J \times K}$, Tri-Planar Decomposition factorises \mathcal{T} such that for a given ijk index position within \mathcal{T} :

$$\mathcal{T}_{ijk} = \sum_{r=1}^R \mathbf{P}_{r,ij}^{XY} \circ \mathbf{P}_{r,jk}^{YZ} \circ \mathbf{P}_{r,ik}^{XZ} \quad (1)$$

where \circ is either the sum (shown in Fig. 1) or product. In preliminary results, we found that the product performs better, so exclusively used it throughout this work. $\mathbf{P}_r^{XY} \in \mathbb{R}^{I \times J}$, $\mathbf{P}_r^{YZ} \in \mathbb{R}^{J \times K}$, $\mathbf{P}_r^{XZ} \in \mathbb{R}^{I \times K}$ are the factorised 2D planes for the r^{th} component. R is the rank of the decomposition, and is a user-selected hyper-parameter. Increasing R improves the accuracy of the decomposition, but at the expense of memory and computation time. Explicit representation utilises a 4D Tensor $\mathbf{V} \in \mathbb{R}^{H \times W \times D \times C}$ with $C \geq 1$. However since $C \ll H, W, D$, for simplicity the Channel dimension is not decomposed

and instead Eq. (1) is repeated C times. Eq. (1) can also be evaluated at non-integer ijk indices by bilinearly interpolating within each tri-plane.

3.2.1 CP Decomposition:

Given the same 3D Tensor $\mathcal{T} \in \mathbb{R}^{I \times J \times K}$, CP Decomposition factorises \mathcal{T} such that for a given ijk index:

$$\mathcal{T}_{ijk} = \sum_{r=1}^R \mathbf{v}_{r,i}^X \mathbf{v}_{r,j}^Y \mathbf{v}_{r,k}^Z \quad (2)$$

where $\mathbf{v}_r^X \in \mathbb{R}^I, \mathbf{v}_r^Y \in \mathbb{R}^J, \mathbf{v}_r^Z \in \mathbb{R}^K$ are the factorised 1D vectors for the r^{th} component. As before, R is the rank and is user-selected, and Eq. (2) is repeated for each Channel in \mathbf{V} . Non-integer indices can also be used by linearly interpolating. Both Eqs. (1) and (2) can be visualised in Fig. 1.

3.3 Pipeline of RapidVol

To form \mathbf{V} from a set of 2D ultrasound freehand scans (Π) with known poses Λ , RapidVol undergoes the following steps (as shown in Fig. 2):

1. The pose (parameterised by \mathbf{E} and \mathbf{T}) of each image is used to construct a grid $G = \{\mathbf{x}_i\}_{i=1}^n = \{x_i, y_i, z_i\}_{i=1}^n$ of a nominated resolution, which contains the 3D co-ordinates of all n pixels which lie on that cross-sectional plane/image.

2. G is fed into our reconstruction model, which performs either Eq. (1) or Eq. (2) on each \mathbf{x}_i . This in turn produces a grid of the same shape as G , but now with C channels rather than 1. Positional encoding (see Appendix A or [12]) is then applied on this grid, before being fed into the MLP.

3. A lightweight, trainable MLP decodes the positionally encoded grid of C channels to 1 channel, resulting in a grayscale image of the fetal brain at the requested pose.

4. The loss, chosen to be the negative Structural Similarity Index Measure (SSIM) [22] between the rendered image and the ground truth image, is computed. Using standard back-propagation the tri-planes (or tri-vectors) are then refined, as is the decoder MLP and optionally the poses of the training images.

Once the brain is reconstructed, cross-sectional views at any pose can be viewed simply by specifying the pose and performing steps 1-3 above.

4 Experimental Setup

4.1 Technical Details

Dataset: Throughout, we use a set of 3D ultrasound fetal brain scans at 20 gestational weeks of size 160^3 voxels, with a resolution of 0.6 mm^3 isotropic, collected as part of the INTERGROWTH-21st study [16]. In practice, only a set of N freehand 2D images are required for reconstruction. However to

evaluate the accuracy of our reconstruction method, we also require a 3D scan of the fetus so that we can compare an arbitrary plane from the reconstructed volume to the ground truth (extracted from the 3D scan). For each fetus we only had a 3D scan, rather than a 3D scan *and* a series of freehand images, so we had to mimic the latter. This was done by sampling N linearly spaced axial images from the 3D scan, which simulates the ultrasound probe moving along the stomach from head to toe during a typical prenatal scanning session. Π was then those N images, and Λ was their (ground truth) poses. When evaluating the accuracy of our reconstruction, views at those poses were naturally not requested.

Implementation Details: We implement our framework in PyTorch. Unless otherwise stated, the tri-planes/tri-vectors are randomly initialised. A Stochastic Gradient Descent (SGD) optimiser with a learning rate (lr) of 0.5 is used to refine the decomposition/reconstruction model, and a SGD with a lr of 0.001 for the decoder MLP. Training is done for 5,000 epochs.

4.2 Experiments Performed

Ablation Study: We first performed an ablation study to find the optimum type of decomposition (Tri-Planar or CP), MLP (see Fig. 2), as well as the degree to positionally encode up to, and whether the raw input should be concatenated with the encoded input or not. The MLPs ablated over all had input size C , output size 1, and were two to four layers, with hidden layers being of size $\{32,64,128\}$. ReLU activation functions were used, except on the final layer which had a sigmoid activation function to constrain the output to be a grasyscale value between 0.0 and 1.0.

Performance Comparison: We then compared the performance, both in terms of reconstruction accuracy and speed, of our method to a state-of-the-art reconstruction method, ImplicitVol [24], on 15 3D fetal brains. Two different sets of input scans Π were used: The first was a set of $N = \{128, 256\}$ axial slices as previously described (Π_1), the second was a set of $N = \{128, 256\}$ coronal slices uniformly rotated 360° about the Vertical Axis of the brain (Π_2). This is to simulate the ultrasound probe being rotated by hand as is often done in a prenatal scan, and is the same dataset used in [24]. Reconstruction accuracy was quantified by requesting views of $N = \{128, 256\}$ linearly spaced axial, coronal and sagittal slices.

Training from an Atlas: Additionally, we investigated whether the reconstruction of a 20 week old fetal brain could be sped up by initialising the tri-planes/tri-vectors from an atlas of the same age, rather than from random values. This atlas was a pre-computed reconstruction of multiple fetal brains. All fetuses were of the same age, and the 3D scans of their brains were deemed to be of high enough quality to be used in constructing a digital atlas for that gestational week [15].

Use of Inaccurate Poses: Ordinarily, we mimicked the set of input freehand scans Π by sampling N images from a 3D scan, and so we knew their ground truth poses which is what we set Λ to be. However in practice, the poses of the freehand images are unknown, so we require methods like PlaneInVol [23] to predict them. Unfortunately neither the dataset used to train PlaneInVol nor a fully trained version of PlaneInVol is publicly available. In this experiment, we instead set Λ to be the ground truth poses plus some random noise ($X \sim U(-3, 3)$), to simulate the inevitably inaccurate pose estimation of PlaneInVol. The poses were also set to be learnable, so as training progressed, the poses could tend towards their ground truth values and reconstruction became more accurate. The poses were refined using an Adam optimiser with a learning rate of 0.001. Optimisation of the poses was done jointly with optimisation of the tri-planes and MLP, as in [24].

5 Results and Discussion

Ablation Study: CP decomposition, although quicker and more memory efficient than Tri-Planar Decomposition, was found to be *too* simple to accurately reconstruct the intricate 3D fetal brain (see Appendix B). A two-layer MLP with a hidden layer size of 64 (as used in [14]), alongside positional encoding to degree $L = 2$ and concatenating the raw input with the encoded input, performed the best (see Appendix B). For this MLP, it was found that the best compromise between accuracy, speed and memory storage was when Tri-Planar Decomposition was performed with $R = 5$ and $C = 10$. Therefore all subsequent experiments used Tri-Planar Decomposition with these parameters.

Performance Comparison: Table 1 shows the reconstruction performance of RapidVol compared to current state of the art, ImplicitVol. If Π is a series of scans acquired by rotating an US probe by hand (Π_2), then our method is more accurate than ImplicitVol at generating novel cross-sectional views, but only marginally so. Nevertheless it still remains significantly quicker. However if it is instead given a series of axial scans (Π_1), then our method is just as quick as with Π_2 , but also on average 41% more accurate. RapidVol therefore prefers if US scans are acquired through longitudinal sweeps as opposed to

Table 1: Evaluation of -SSIM accuracy results at test time for our method (RapidVol) vs the baseline (ImplicitVol) on 15, 20 week fetal brains. More negative SSIM is better.

Π	Method	N = 128 Testing Slices			N = 256 Testing Slices		
		Axial	Coronal	Sagittal	Axial	Coronal	Sagittal
Axial	RapidVol	N/A	-0.955±0.008	-0.952±0.009	N/A	-0.973±0.005	-0.969±0.006
	ImplicitVol	N/A	-0.689±0.038	-0.700±0.046	N/A	-0.677±0.040	-0.662±0.037
360° Coronal	RapidVol	-0.941±0.016	-0.932±0.018	-0.935±0.017	-0.952±0.015	-0.950±0.016	-0.950±0.014
	ImplicitVol	-0.909±0.021	-0.901±0.023	-0.905±0.022	-0.912±0.020	-0.904±0.023	-0.908±0.022

rotational sweeps of the probe, both of which are readily available. Regardless of the acquisition technique, our method performs better when given more input scans. Since 2D US acquires images in real-time, collecting hundreds of images is quick and effortless, so the quality of the 3D reconstruction can easily be improved. Finally, our method generates novel views equally well in all three orthogonal planes, regardless of the acquisition technique used. Their accuracy is also much less variable from fetus to fetus than ImplicitVol (c.f standard deviations in Table 1).

All runs were conducted on a shared high-performance cluster, however pre-emption by other processes often occurred. Therefore to ensure a fair timing comparison between RapidVol and ImplicitVol, a selection of these runs were made on a much slower, but *isolated* GPU (GTX TITAN X). The results of the *relative* speed up, as well as the training profiles, can be seen in Fig. 3, showing that RapidVol is 3 times quicker than ImplicitVol per epoch. This significant speed-up, coupled with the accuracy improvements discussed above, makes for a very powerful reconstruction model. This experiment was run on a slow GPU, so upon deployment onto an isolated modern GPU, the absolute reconstruction/training time will be in the order of minutes as opposed to over 1 hour as shown in Fig. 3.

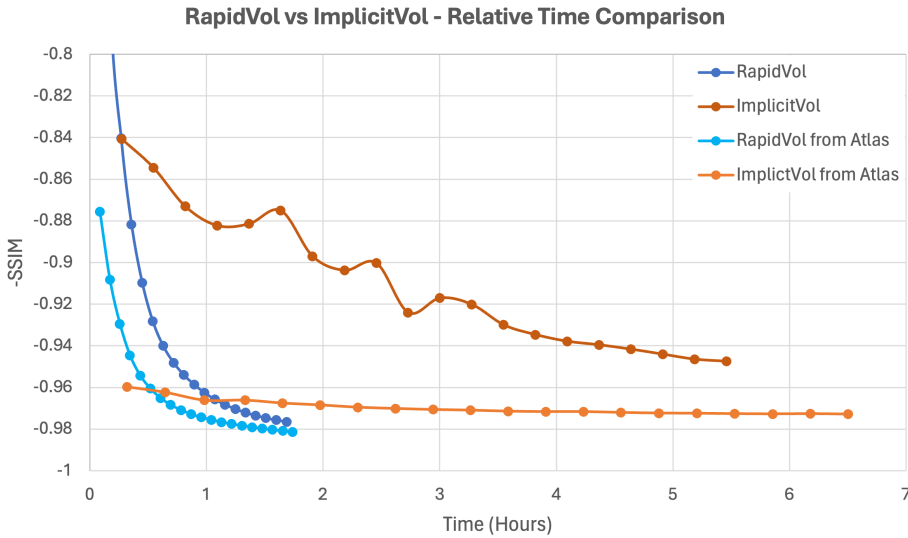


Figure 3: Testing accuracy profile curves. Training was done to 5,000 epochs, accuracy reported every 250 epochs. For consistent timings, these runs were done on an isolated but much slower GPU. $\Pi = 160$ axial slices, Testing dataset = 160 coronal slices rotated 360° about the Vertical Axis.

Training from an Atlas: Fig. 3 shows that initialising from a pre-trained fetal brain atlas as opposed to randomly has no effect on reconstruction speed. It does however result in a far quicker rate of convergence, which is especially useful if the reconstruction process is required to be terminated after a certain duration (e.g. a 30 minute prenatal appointment). To create a reconstructed brain with a respectable SSIM of 0.9, initialising RapidVol from an atlas allows you to achieve this 2.7 times quicker than if RapidVol was initialised from random values. We therefore recommend all fetal brains are reconstructed using RapidVol which has been pre-initialised from a digital fetal atlas of the same age (these digital atlases are publicly available for most gestational ages [15]).

Use of Inaccurate Poses: Table 2 shows that as expected, inaccurate poses lead to poorer reconstruction accuracy, regardless of the method. However when faced with inaccurate poses, which in practice will always be the case to some extent, our method is up to 35% more accurate than the baseline. Even when a series of parallel sagittal poses are requested, we still perform 28% better, demonstrating the robustness of our proposed method.

Table 2: -SSIM accuracy results at test time, when our method does or does not have accurate initial poses. $\Pi = 256$ coronal slices rotated 360° about the Vertical Axis. Testing dataset = 256 {axial, coronal, sagittal} slices. More negative SSIM is better.

Poses	Method	Axial	Coronal	Sagittal
Ground Truth	RapidVol	-0.952	-0.950	-0.950
	ImplicitVol	-0.912	-0.904	-0.908
Estimated	RapidVol	-0.812	-0.790	-0.790
	ImplicitVol	-0.599	-0.596	-0.616

6 Conclusion

We propose **RapidVol**, a hybrid implicit-explicit representation method utilising Tri-Planar Decomposition to rapidly reconstruct 3D ultrasound volumes from sensorless 2D scans. When compared to current state of the art, our method is up to 3x quicker, up to 46% more accurate, and even if faced with slightly inaccurate poses is still robust, performing on average 32% better than other methods do in that scenario. Reconstructing from a fetal atlas can also offer further speed-up. RapidVol helps to bring us one step closer to more efficient and accurate medical diagnostics, especially in settings where only basic 2D US probes are available but 3D views would be clinically beneficial.

Acknowledgements. The authors acknowledge the generous support of the EPSRC Centre for Doctoral Training in Autonomous Intelligent Machines & Systems (EP/S024050/1), Amazon Web Services, EPSRC Impact Acceleration Account Award, EPSRC Doctoral Prize Scheme, Royal Academy of Engineering (RF\201819\18\163), and the Bill & Melinda Gates Foundation.

References

- [1] Campbell, S.: Prenatal ultrasound examination of the secondary palate. *Ultrasound in Obstetrics & Gynecology* **29**(2), 124–127 (2007). <https://doi.org/10.1002/uog.3954>
- [2] Carroll, J.D., Chang, J.J.: Analysis of individual differences in multidimensional scaling via an n-way generalization of “Eckart-Young” decomposition. *Psychometrika* **35**(3), 283–319 (Sep 1970). <https://doi.org/10.1007/BF02310791>
- [3] Chan, E.R., Lin, C.Z., Chan, M.A., Nagano, K., Pan, B., De Mello, S., Gallo, O., Guibas, L., Tremblay, J., Khamis, S., Karras, T., Wetzstein, G.: Efficient Geometry-aware 3D Generative Adversarial Networks. In: 2022 IEEE/CVF Conference on Computer Vision and Pattern Recognition (CVPR). pp. 16102–16112. IEEE, New Orleans, LA, USA (Jun 2022). <https://doi.org/10.1109/CVPR52688.2022.01565>
- [4] Chen, A., Xu, Z., Geiger, A., Yu, J., Su, H.: TensorRF: Tensorial Radiance Fields (Nov 2022), [arXiv:2203.09517](https://arxiv.org/abs/2203.09517) [cs]
- [5] Chen, A., Xu, Z., Zhao, F., Zhang, X., Xiang, F., Yu, J., Su, H.: MVS-NeRF: Fast Generalizable Radiance Field Reconstruction from Multi-View Stereo (Aug 2021), [arXiv:2103.15595](https://arxiv.org/abs/2103.15595) [cs]
- [6] Chen, M.L., Chang, C.H., Yu, C.H., Cheng, Y.C., Chang, F.M.: Prenatal diagnosis of cleft palate by three-dimensional ultrasound. *Ultrasound in Medicine and Biology* **27**(8), 1017–1023 (Aug 2001). [https://doi.org/10.1016/S0301-5629\(01\)00403-3](https://doi.org/10.1016/S0301-5629(01)00403-3), publisher: Elsevier
- [7] Flynn, J., Broxton, M., Debevec, P., DuVall, M., Fyffe, G., Overbeck, R., Snavely, N., Tucker, R.: DeepView: View Synthesis with Learned Gradient Descent (Jun 2019), [arXiv:1906.07316](https://arxiv.org/abs/1906.07316) [cs, eess]
- [8] Gonçalves, L.F.: Three-dimensional ultrasound of the fetus: how does it help? *Pediatric Radiology* **46**(2), 177–189 (Feb 2016). <https://doi.org/10.1007/s00247-015-3441-6>
- [9] Henzler, P., Rasche, V., Ropinski, T., Ritschel, T.: Single-image Tomography: 3D Volumes from 2D Cranial X-Rays (Nov 2018), [arXiv:1710.04867](https://arxiv.org/abs/1710.04867) [cs]
- [10] Huang, Q., Zeng, Z.: A Review on Real-Time 3D Ultrasound Imaging Technology. *BioMed Research International* **2017**, 1–20 (2017). <https://doi.org/10.1155/2017/6027029>

- [11] Merz, E., Pashaj, S.: Advantages of 3D ultrasound in the assessment of fetal abnormalities. *Journal of Perinatal Medicine* **45**(6), 643–650 (Aug 2017). <https://doi.org/10.1515/jpm-2016-0379>, publisher: De Gruyter
- [12] Mildenhall, B., Srinivasan, P.P., Tancik, M., Barron, J.T., Ramamoorthi, R., Ng, R.: NeRF: Representing Scenes as Neural Radiance Fields for View Synthesis (Aug 2020), arXiv:2003.08934 [cs]
- [13] Mohamed, F., Vei Siang, C.: A Survey on 3D Ultrasound Reconstruction Techniques. In: Antonio Aceves-Fernandez, M. (ed.) *Artificial Intelligence - Applications in Medicine and Biology*. IntechOpen (Jul 2019). <https://doi.org/10.5772/intechopen.81628>
- [14] Müller, T., Evans, A., Schied, C., Keller, A.: Instant neural graphics primitives with a multiresolution hash encoding. *ACM Transactions on Graphics* **41**(4), 1–15 (Jul 2022). <https://doi.org/10.1145/3528223.3530127>
- [15] Namburete, A.I.L., Papież, B.W., Fernandes, M., Wyburd, M.K., Hesse, L.S., Moser, F.A., Ismail, L.C., Gunier, R.B., Squier, W., Ohuma, E.O., Carvalho, M., Jaffer, Y., Gravett, M., Wu, Q., Lambert, A., Winsey, A., Restrepo-Méndez, M.C., Bertino, E., Purwar, M., Barros, F.C., Stein, A., Noble, J.A., Molnár, Z., Jenkinson, M., Bhutta, Z.A., Papageorghiou, A.T., Villar, J., Kennedy, S.H.: Normative spatiotemporal fetal brain maturation with satisfactory development at 2 years. *Nature* pp. 1–9 (Oct 2023). <https://doi.org/10.1038/s41586-023-06630-3>, publisher: Nature Publishing Group
- [16] Papageorghiou, A.T., Ohuma, E.O., Altman, D.G., Todros, T., Ismail, L.C., Lambert, A., Jaffer, Y.A., Bertino, E., Gravett, M.G., Purwar, M., Noble, J.A., Pang, R., Victora, C.G., Barros, F.C., Carvalho, M., Salomon, L.J., Bhutta, Z.A., Kennedy, S.H., Villar, J.: International standards for fetal growth based on serial ultrasound measurements: the Fetal Growth Longitudinal Study of the INTERGROWTH-21st Project. *The Lancet* **384**(9946), 869–879 (Sep 2014). [https://doi.org/10.1016/S0140-6736\(14\)61490-2](https://doi.org/10.1016/S0140-6736(14)61490-2), publisher: Elsevier
- [17] Pistorius, L.R., Stoutenbeek, P., Groenendaal, F., de Vries, L., Manten, G., Mulder, E., Visser, G.: Grade and symmetry of normal fetal cortical development: a longitudinal two- and three-dimensional ultrasound study. *Ultrasound in Obstetrics & Gynecology* **36**(6), 700–708 (2010). <https://doi.org/10.1002/uog.7705>
- [18] Seitz, S., Dyer, C.: Photorealistic scene reconstruction by voxel coloring. In: *Proceedings of IEEE Computer Society Conference on Computer Vision and Pattern Recognition*. pp. 1067–1073. IEEE Comput. Soc, San Juan, Puerto Rico (1997). <https://doi.org/10.1109/CVPR.1997.609462>

- [19] Shalma, H., Selvaraj, P.: A review on 3D image reconstruction on specific and generic objects. *Materials Today: Proceedings* **80**, 2400–2405 (Jan 2023). <https://doi.org/10.1016/j.matpr.2021.06.371>
- [20] Szeliski, R., Golland, P.: Stereo matching with transparency and matting. In: *Sixth International Conference on Computer Vision (IEEE Cat. No.98CH36271)*. pp. 517–524. Narosa Publishing House, Bombay, India (1998). <https://doi.org/10.1109/ICCV.1998.710766>
- [21] Tang, J., Chen, X., Wang, J., Zeng, G.: Compressible-composable NeRF via Rank-residual Decomposition (Oct 2022), arXiv:2205.14870 [cs]
- [22] Wang, Z., Bovik, A., Sheikh, H., Simoncelli, E.: Image Quality Assessment: From Error Visibility to Structural Similarity. *IEEE Transactions on Image Processing* **13**(4), 600–612 (Apr 2004). <https://doi.org/10.1109/TIP.2003.819861>
- [23] Yeung, P.H., Aliasi, M., Papageorghiou, A.T., Haak, M., Xie, W., Namburete, A.I.L.: Learning to map 2D ultrasound images into 3D space with minimal human annotation. *Medical Image Analysis* **70**, 101998 (May 2021). <https://doi.org/10.1016/j.media.2021.101998>
- [24] Yeung, P.H., Hesse, L., Aliasi, M., Haak, M., Consortium, t.I.s., Xie, W., Namburete, A.I.L.: ImplicitVol: Sensorless 3D Ultrasound Reconstruction with Deep Implicit Representation (Sep 2021), arXiv:2109.12108 [cs, eess]
- [25] Yu, A., Fridovich-Keil, S., Tancik, M., Chen, Q., Recht, B., Kanazawa, A.: Plenoxels: Radiance Fields without Neural Networks (Dec 2021), arXiv:2112.05131 [cs]
- [26] Zhou, T., Tucker, R., Flynn, J., Fyffe, G., Snavely, N.: Stereo Magnification: Learning View Synthesis using Multiplane Images (May 2018), arXiv:1805.09817 [cs]

Appendix A - Positional Encoding

Each element in feature vector \mathbf{p} is encoded from \mathbb{R} to \mathbb{R}^{2L+1} by the following function:

$$\gamma(p) = (p, \sin(2^0\pi p), \cos(2^0\pi p), \dots, \sin(2^{L-1}\pi p), \cos(2^{L-1}\pi p)) \quad (\text{A1})$$

The degree of encoding (ie value of L), and whether or not to include p itself in $\gamma(p)$, are application specific choices.

Appendix B - Ablation Study

Table B1: Comparison between possible RapidVol setups. L = positional encoding degree. “+ input” = concatenate raw input with encoded input. Tri-Planar and CP Decomposition are both with Rank $R = 5$, Channels $C = 10$. Reconstruction is from 160 linearly spaced axial images. Testing dataset is 160 linearly spaced coronal slices. Values shown are reconstruction accuracy as measured with Negative SSIM (more negative is better). The best result for each network is shown in bold, with the overall best performance across the networks underlined. Network names are of the form “MLP n - w ”. This stands for a Multilayer Perceptron (MLP) network with n fully connected layers, and hidden layer(s) all of width w . ReLU activation functions are used throughout, except for the last layer which has a sigmoid activation function.

Network		$L = 0$	$L = 2$	$L = 5$	$L = 10$	$L = 2$ + input	$L = 5$ + input	$L = 10$ + input
Tri-Planar	MLP 2-128	-0.9568	-0.9717	-0.2573	-0.2630	-0.9733	-0.2608	-0.9303
	MLP 3-128	-0.9647	-0.9743	-0.2591	-0.3055	-0.9748	-0.2623	-0.9243
	MLP 4-128	-0.9709	-0.9745	-0.2617	-0.8803	-0.9750	-0.2635	-0.9403
	MLP 3-32	-0.9641	-0.9744	-0.2567	-0.9341	-0.9758	-0.2636	-0.9227
	MLP 3-64	-0.9654	-0.9738	-0.2583	-0.8738	-0.9743	-0.2632	-0.9307
	MLP 2-64	-0.9562	-0.9729	-0.2556	-0.8448	<u>-0.9764</u>	-0.2609	-0.9167
CP + MLP 2-64	-0.8544	-0.8475	-0.8265	NaN	-0.8512	-0.8392	-0.508	